Supramolecular Chemistry

International Edition: DOI: 10.1002/anie.201411462
German Edition: DOI: 10.1002/ange.201411462

Formation of a Fluorous/Organic Biphasic Supramolecular Octopus Assembly for Enhanced Porphyrin Phosphorescence in Air**

Chi Yang, Ravi K. Arvapally, Sammer M. Tekarli, Gustavo A. Salazar, Oussama Elbjeirami†, Xiaoping Wang, and Mohammad A. Omary**

Dedicated to Professor Jingzhang Gao and Professor Yuan Wang

Abstract: *The trinuclear triangle-shaped system [tris{3,5-bis(heptafluoropropyl)-1,2,4-triazolatosilver(I)}] (**1**) and the multi-armed square-shaped metalloporphyrin PtOEP or the free porphyrin base H_2OEP serve as excellent octopus hosts (OEP = 2,3,7,8,12,13,17,18-octaethyl-21H,23H-porphine). Coupling of the fluorous/organic molecular octopi **1** and H_2OEP or PtOEP by strong quadrupole–quadrupole and metal–π interactions affords the supramolecular assemblies [**1**·PtOEP] or [**1**·H_2OEP] (**2a**), which feature nanoscopic cavities surrounding the upper triangular and lower square cores. The fluorous/organic biphasic configuration of [**1**·PtOEP] leads to an increase in the phosphorescence of PtOEP under ambient conditions. Guest molecules can be included in the biphasic double-octopus assembly in three different site-selective modes.*

Self-assembly of octopus arms around a guest molecule is a powerful strategy to obtain architectures in which the steric and electronic properties of the shell control the guest environment.[1] Octopus molecules represent a class of molecular hosts composed of a rigid core with multiple surrounding flexible substituents. A variety of octopus hosts have been explored since the pioneering work of Vögtle and co-workers.[1] On the other hand, π–π and metal–π interactions between an octopus core and an aromatic guest may act as driving forces towards an ordered one-dimensional (1D) octopus-like supramolecular array. Numerous 1D π-stacked and/or metal-mediated supramolecular polymers have been reported in the last decade.[2] The use of fluorous octopus arms may induce novel functions akin to those enabled by fluorous metal–organic frameworks (FMOFs)[3,4] or non-porous analogues thereof that bear fluorous surfaces.[5] The monovalent Ag^I, Au^I, and Cu^I salts of 1,2,4-triazolate (Tz) readily assemble into discrete trinuclear macrocycles, $[M_3(Tz)_3]$,[6] which can serve as the octopus core while the six 3,5-substituents serve as flexible octopus arms.[7,8] The electronic and chemical properties of fluorous $[M_3Tz_3]$-based octopus complexes are easily tunable using triazole chemistry. This work and parallel prior studies by Dias et al. and our group show that a fluorous octopus such as $[Ag_3(\mu^{1,2}\text{-}3,5\text{-}(n\text{-}C_3F_7)_2Tz)_3]$ (**1**) can be constructed and has excellent inclusion and optoelectronic properties.[9]

Herein, we show that fluorous octopus **1** can be combined with porphyrin octopi to form biphasic double-octopus assemblies with fluorous and non-fluorous arms on opposite sides; the corresponding nanoscopic phases thus display interesting inclusion properties. The metalloporphyrin PtOEP and the free porphyrin base H_2OEP (OEP = 2,3,7,8,12,13,17,18-octaethyl-21*H*,23*H*-porphine) were selected because of their wide-ranging applications.[10–12] DFT calculations showed that the molecular electrostatic potentials (MEPs) of H_2OEP and PtOEP exhibit an electron-rich (π-basic) region at the center of the squares whereas $[Ag_3(\mu^{1,2}\text{-}3,5\text{-}(n\text{-}C_3F_7)_2Tz)_3]$ (**1**) is very electron-poor (strongly π-acidic) at the center of the nine-membered ring (Scheme 1b). The electron-rich regions in H_2OEP and PtOEP are susceptible to quadrupole–quadrupole interactions with the strongly electron-deficient region of **1**. The difference between the Q_{zz} values of **1** (+20) and the porphyrin systems (−24 for H_2OEP; −30 for PtOEP) accentuates strong attractive interactions, which assist π–π and/or metal–π forces in the formation of the stacked pairs [**1**·H_2OEP] (**2a**) and [**1**·PtOEP] (**2**).

The reaction of **1** with PtOEP or H_2OEP in dichloromethane or benzene afforded double-octopus assembly **2** or **2a** in high yield. Both **2** and **2a** can be recrystallized from benzene to give red $[\mathbf{2}\cdot(C_6H_6)_{1.5}]$ or dark-purple $[\mathbf{2a}\cdot(C_6H_6)]$ crystals. **2a** crystallizes in the triclinic space group $P\bar{1}$ as a discrete [**1**·H_2OEP] pair (Figure 1) with one benzene molecule per asymmetric unit. The adduct pair consists of

[*] Prof. Dr. C. Yang, Dr. R. K. Arvapally, Dr. S. M. Tekarli, G. A. Salazar, Dr. O. Elbjeirami, Dr. X. Wang, Prof. Dr. M. A. Omary
Department of Chemistry, University of North Texas
Denton, TX 76203 (USA)
E-mail: chi.yang@unt.edu
omary@unt.edu
Dr. S. M. Tekarli
Department of Chemistry, Collin College
Plano, Texas 75074 (USA)
Dr. X. Wang
Chemical and Engineering Materials Division
Oak Ridge National Laboratory
Oak Ridge, Tennessee 37831 (USA)
[†] Deceased.

[**] Support by the U.S. National Science Foundation (CHE-1413641, CHE-0911690, CMMI-0963509, and CHE-0840518) and the Robert A. Welch Foundation (Grant B-1542) is gratefully acknowledged. X.P.W. acknowledges support by the Scientific User Facilities Division, Office of Basic Energy Sciences, U.S. Department of Energy (DE-AC05-00OR22725) managed by UT Battelle, LLC.
Supporting information for this article is available on the WWW under http://dx.doi.org/10.1002/anie.201411462.

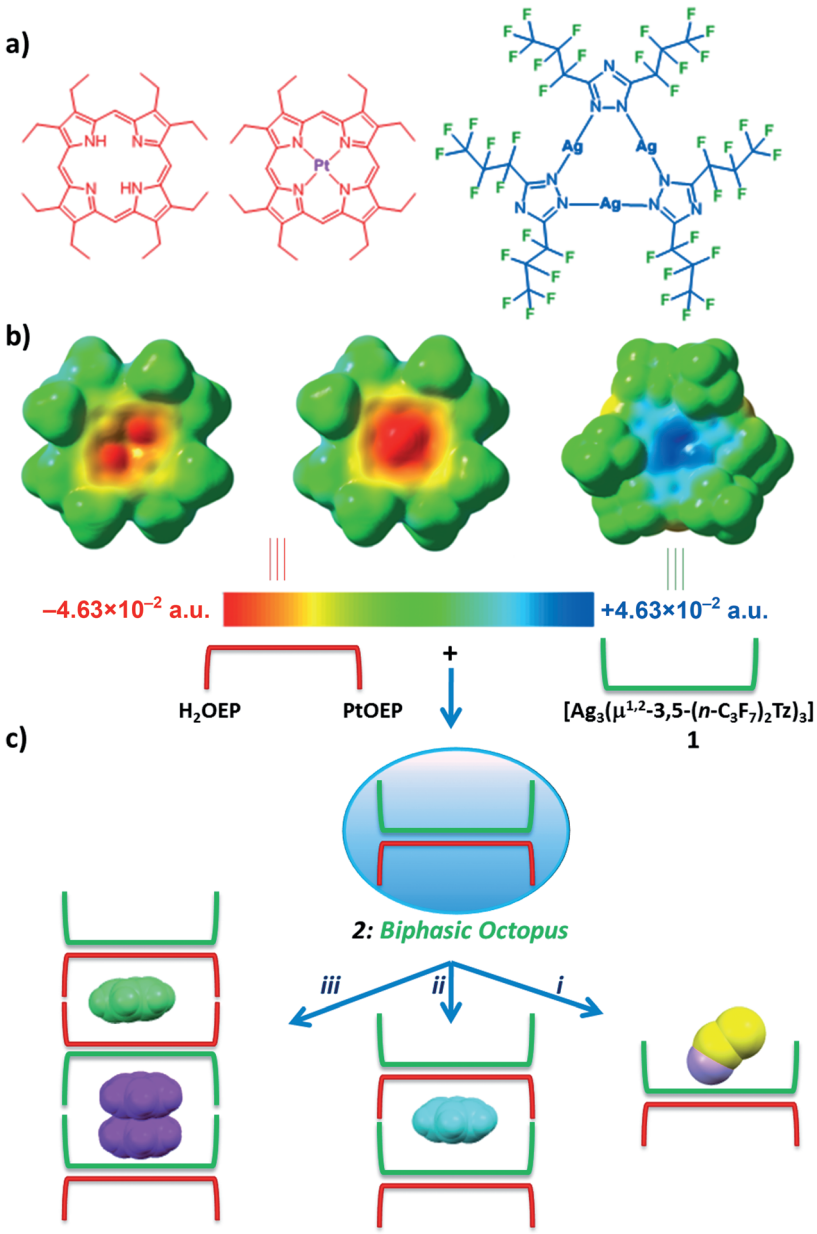

Scheme 1. a, b) Chemical structure (a) and MEPs (b) of H_2OEP, PtOEP, and **1** mapped on the electron density surfaces. c) Formation of biphasic double-octopus assembly **2** by quadrupole–quadrupole interactions. Three different guest-inclusion modes are possible: i) head-on inclusion of a linear guest within the fluorous cavity; ii) inclusion of an aromatic guest within the nest consisting of a semi-fluorous phase and a semi-organic phase; iii) inclusion of an aromatic π-dimer within the fluorous cage while an aromatic monomer is included within the organic cage. The MEP values are plotted on a scale ranging from -4.63×10^{-2} a.u. (red-most values; a.u. = atomic units) to $+4.63\times10^{-2}$ a.u. (blue-most values).

fluorous bowl-shaped **1** and H_2OEP, which are held together by coordination, π-stacking (quadrupole–quadrupole), and van der Waals forces. In this rare type of Ag_3–porphyrin bonding, the imino hydrogen atoms are located on one pair of pyrrole N atoms in the porphyrin. The unprotonated N11/N13 atoms and the Ag_3 cluster were found to strongly interact, with interatomic distances of 2.53 Å (Ag3–N11) and 2.95 Å (Ag1–N13). The shorter Ag3–N11 distance is comparable with those reported for supramolecular arrays of Ag^I–polypyridines (2.15–2.55 Å),[2d–f] and shorter than the axial Ag–N(Tz) bond (2.62 Å) found in FMOF-1.[4] The strong interaction between the porphyrin ring of H_2OEP and Ag_3 cluster **1** is such that the Ag atoms protrude out of the plane of the three Tz rings, with maximum vertical displacements of the silver(I) atoms from the plane of the six N atoms of 0.33 (Ag1), 0.10 (Ag2), and 0.63 Å (Ag3). Remarkably, the two unprotonated N atoms that are bonded to the Ag_3 cluster also protrude out of the porphyrin mean plane, with a vertical distance to the porphyrin plane of 0.12 (N11) and 0.10 Å (N13). DFT calculations gave a binding energy of 62.06 kcal mol^{-1} for **2a**, indicating that the Ag_3–porphyrin bonding is strengthened by electrostatic quadrupolar interactions between **1** and H_2OEP (Supporting Information, Figure S2). The [**1**·H_2OEP] pair is stabilized by an octopus shell formed by six perfluoroalkyl *n*-C_3F_7 arms oriented upwards to provide a fluorine-lined electron-poor cavity above the stack; eight C_2H_5 arms are oriented downwards to afford a hydrogen-lined electron-rich cavity below the stack, which renders the adduct polar, asymmetric, and biconcave. The [**1**·H_2OEP] units are packed along the *a* axis such that the fluorine-lined bowl and the hydrogen-lined bowl are glued together to form a benzene-encapsulating supramolecular cage (Scheme 1c, ii).

Biphasic double-octopus **2** crystallizes in the monoclinic space group *P*21/*c* as two crystallographically independent [**1**·PtOEP] pairs (Figure 1, right) along with three crystallographically independent benzene molecules in the asymmetric unit. The 1:1 cofacial adduct **2** adopts a similar biconcave conformation as **2a**, except that the face-to-face overlap in [**1**·PtOEP] is strengthened by donor–acceptor Pt–Ag metallophilic bonding. The shortest Pt–Ag and Pt–Ag_3 centroid distances in **2** are 3.040 and 2.847 Å, respectively, which fall in the range of Pt–Ag dative-bond distances reported in the literature (2.7–3.2 Å).[13a,b] The binding energy of **2** was determined to be 67.81 kcal mol^{-1} by DFT calculations, which indicates that the Pt→Ag metallophilic/dative bond is strengthened by electrostatic quadrupolar interactions between **1** and PtOEP (Figure S2). The quadrupolar interactions in **2** and **2a** are stronger than those in the non-octopus adduct [{Au(bzim)}$_3$]/[{Hg(C_6F_4)}$_3$], which was reported by Burini and co-workers (bzim = 1-benzylimidazolate; see the Supporting Information).[13c]

The asymmetric units in **2** are related by a two-fold axis such that a one-dimensional array of stacked chromophores

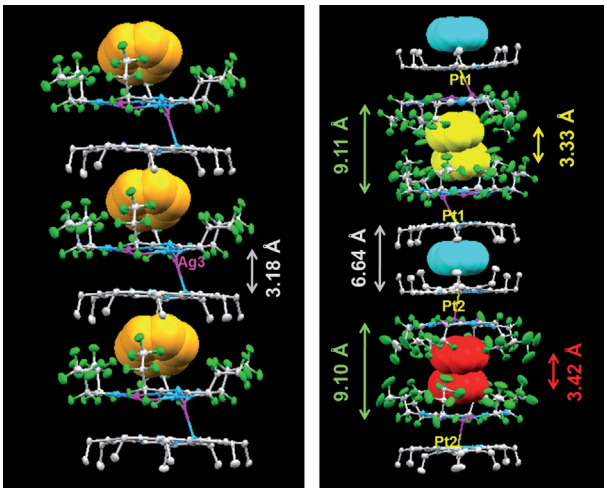

Figure 1. Illustration of infinite π-stacks in crystals of [**2a**·C_6H_6] and [**2**·$C(C_6H_6)_{1.5}$] along the *a* and *c** axes, respectively. The three independent benzene molecules in [**2**·$C(C_6H_6)_{1.5}$] are indicated as red, blue, and yellow space-filling spheres.

with alternating benzene–**1**–PtOEP–benzene–PtOEP–**1**–benzene units is generated along the *c** axis (Figure 1b). Aside from Pt–Ag metallophilic and electrostatic/quadrupolar forces, the extended stacking is mediated by π–π interactions between adjacent chromophores, including those between benzene–benzene, benzene–**1**, **1**–PtOEP, and PtOEP–benzene units (interplanar angles of 0, 12.7, 1.1, and 3.3°, respectively), resulting in pair-wise separations of 3.33, 6.64, and 9.11 Å for the benzene–benzene, porphyrin–porphyrin and **1**–**1** pairs, respectively. Such self-assembled aromatic one-dimensional columns that combine metal–metal, π–π, and metal–π interactions favor charge transport along the column chains, favoring applications in organic electronics, for example, in organic photovoltaics (OPVs), light-emitting diodes (OLEDs), and field-effect transistors (OFETs).[14]

One highlight of the stack is the aromatic $(benzene)_2$ π-dimer, which is sandwiched between cofacially stacked macrocycles **1** and enclosed by the fluorine-lined hydrophobic cavity formed by twelve fluorous *n*-C_3F_7 groups. A single benzene molecule is also sandwiched between two cofacial PtOEP planes and is well-nested within a cavity formed by 16 ethyl groups (Scheme 1c, iii). To the best of our knowledge, this is the first example of alternating fluorous/non-fluorous cages formed by cofacially stacked octopus cavities. The biphasic cavities act as host cages to encapsulate π-dimer and monomer guest molecules.

We found that formation of the octopus couple in [**2**·$(C_6H_6)_{1.5}$] can enhance the PtOEP phosphorescence in air. It is well known that pure PtOEP is a very weak emitter in air owing to its extreme sensitivity to O_2 quenching and concentration quenching through a strong bimolecular annihilation process.[10–12] This limitation is a critical bottleneck for the application of PtOEP systems in organic light-emitting devices and full-color displays that require high stability.[15–17] One strategy to circumvent this bottleneck involves the doping of PtOEP into a host matrix of an amorphous organic semiconductor and sealing the device under inert atmosphere.[15] As O_2 quenching of the PtOEP phosphorescence occurs through axial interactions of O_2 with the porphyrin plane and the triplet–triplet annihilation process through intermolecular PtOEP π-interactions, the coupling of PtOEP with a fluorous octopus host effectively protects PtOEP from axial interactions with O_2 and completely prevents the concentration-dependent bimolecular self-annihilation processes.

As seen in Figure 1, the PtOEP molecules in [**2**·$(C_6H_6)_{1.5}$] are well-protected by coupling with **1** under the fluorous shell, which captures invasive guests, such as benzene and O_2. The configuration of [**2**·$(C_6H_6)_{1.5}$] keeps the PtOEP units apart from each other and prevents their interactions with O_2 (which is "filtered" by the fluorous pore).[4a] Electronic spectra of **2** under various conditions are shown in Figure 2a–f. In agreement with its solution absorption spectrum

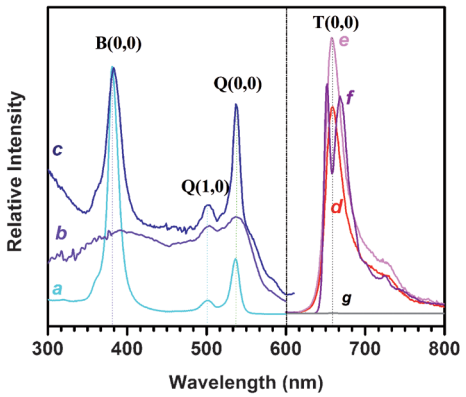

Figure 2. a–c) Solution absorption (a; in CH_2Cl_2), solid-state diffuse reflectance (b), and excitation (c; $\lambda_{em}=660$ nm) spectra of compound **2**. d–f) Luminescence spectra of crystalline **2** ($\lambda_{ex}=540$ nm) in ambient air (d; $\tau=55$ μs), in 100% N_2 (e; $\tau=64$ μs), and at 77 K in air (f; $\tau=93$ μs). g) The gray trace shows the vanishing luminescence of a solid sample of PtOEP under ambient conditions ($\lambda_{ex}=540$ nm) for the same instrument settings.

in CH_2Cl_2, the diffuse reflectance and excitation ($\lambda_{em}=660$ nm) spectra of a solid sample of **2** are governed by the Q- and Soret-band transitions at 380, 502, and 537 nm, which were classified as B(0,0), Q(1,0), and Q(0,0) transitions, respectively.[12,18] Although PtOEP exhibits rather weak emission in air (Figure 2g),[12] crystals of **2** exhibit bright-red luminescence characterized by a porphyrin-based triplet emission at 658 nm [T(0,0)], with weaker emissions at the vibronic harmonic overtones (690 and 720 nm). The solid-state phosphorescence of **2** under ambient conditions exhibits only small intensity increases under oxygen-free conditions (e.g., in pure N_2; Figure 2e), which indicates a rather insensitive response to the presence of O_2 as a result of the well-protected PtOEP sites (see the crystal structure of [**2**·$(C_6H_6)_{1.5}$]; Figure 1). The strong Ag_3–Pt interactions and heavy-atom effects result in a strong sensitization of the doublet T(0,0) band. The lifetime of the phosphorescence of the solid sample of **2** also corroborates the strong sensitization of the PtOEP phosphorescence by the fluorous octopus molecules **1**, as the τ values that we obtained even in ambient

air and at ambient temperature are similar to those measured for PtOEP-doped thin films in inert environments (Figure 2).

Crystals of [**2**·$(C_6H_6)_{1.5}$] remained intact even after standing in air for extended periods of time, suggesting that the benzene molecules are tightly included in the lattice sites. However, when these crystals were exposed to vapors of polar organic solvents, for example, acetone or acetonitrile, the red emission of **2** was significantly quenched. To reveal whether the guest benzene molecules in [**2**·$(C_6H_6)_{1.5}$] played a role in enhancing PtOEP phosphorescence, we replaced them with other solvent molecules. Slow evaporation of a CH_2Cl_2 solution of **2** in the presence of acetonitrile or acetone resulted in non-luminescent dark-red crystals. X-ray analysis showed that these crystals were formed by linear guest inclusion in the biphasic double-octopus system **2** (Scheme 1 c, i) to form [**2**·MeCN] and [**2**·Me_2CO], respectively. The MeCN and Me_2CO solvent molecules were well-nested in the hydrophobic fluorine-lined cavity with head-on coordination to the Ag_3 unit (Figure 3). The corresponding Ag–O(acetone)

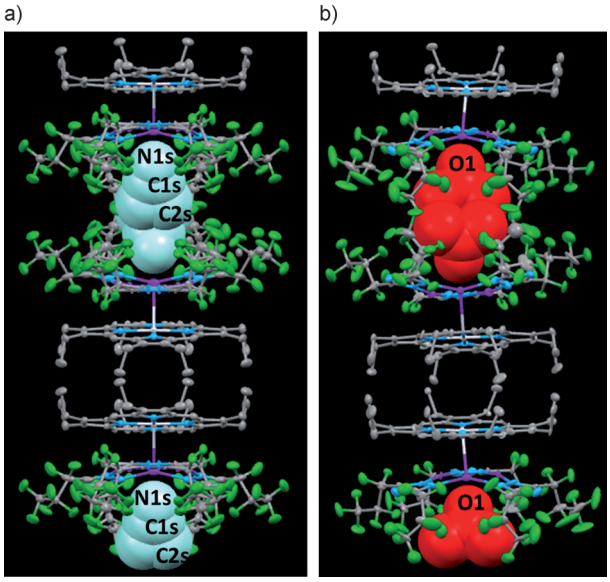

Figure 3. a, b) Crystal packing viewed along the *a* axis in the crystals of [**2**·MeCN] (a) and [**2**·Me_2CO] (b). Acetonitrile and acetone molecules are indicated as light-blue and red space-filling spheres, respectively.

distances were determined to be 2.746, 2.859, and 3.038 Å, and the Ag–N(MeCN) distances were found to be 2.815, 3.134, 3.148 Å with centroid–Ag_3 separations of 2.097 and 2.304 Å for acetone and acetonitrile, respectively.[19,20] These data indicate the presence of strong dipole–quadrupole bonding of acetone and MeCN with Ag_3 in [**2**·Me_2CO] and [**2**·MeCN], respectively, as described in our recent work conducted in collaboration with the Burini and Galassi groups.[21] The strong interactions between the solvent molecules and **2** suggest that the [$Ag_3(\mu^{1,2}$-3,5-(n-$C_3F_7)_2$Tz)$_3$] macrocycles that bear a fluorous octopus shell are strongly Lewis acidic/π-superacidic. An analysis of the crystal packing in [**2**·Me_2CO] and [**2**·MeCN] (Figure 3) revealed small pores between the porphyrin alkyl chains, where gas molecules such as O_2 may reach exposed sides of the porphyrin plane. Such interactions likely represent a principal cause for the emission quenching observed for [**2**·MeCN] and [**2**·Me_2CO] in air, whereas guest inclusion of benzene molecules in [**2**·$(C_6H_6)_{1.5}$] likely plays a sensitizing/protecting role for the PtOEP triplet emission in air. By applying a vacuum to crystals of [**2**·MeCN] and [**2**·Me_2CO] followed by N_2 exposure, the emission of PtOEP was recovered and gave the same emission profile as [**2**·$(C_6H_6)_{1.5}$], which reinforces the aforementioned hypothesis that acetone and acetonitrile inclusion represents a quenching pathway whereas benzene inclusion represents a sensitizing pathway for porphyrin phosphorescence.

In summary, the crystal structures of **2a** and **2** revealed strong electrostatic quadrupole–quadrupole interactions between the electron-deficient Ag_3 macrocycles and the electron-rich free porphyrin base or the metalloporphyrin cores. These interactions acts as important organizational forces in the formation ("self-recognition") of stacked pairs of **1** and the porphyrin systems. The van der Waals interactions between the perfluoroalkyl n-C_3F_7 groups in **1** and the ethyl groups in the porphyrin systems lead to a conformation consisting of a biconcave biphasic octopus pair. The fluorine-lined cavities formed by the octopus-arm-like n-C_3F_7 groups around the Ag_3 cores enhance the chemical, photochemical, and thermal robustness of the immediate metal-cluster environment. In our biphasic octopus assembly, the PtOEP phosphorescence is optimized in two ways as 1) O_2 quenching is effectively prevented and 2) self-quenching and bimolecular triplet–triplet annihilation processes are completely suppressed. Ongoing efforts target "best guest" chromophores for the biphasic octopus couple **2** aside from benzene, such as pyrene, perlene, or coronene, to further optimize the phosphorescence of metalloporphyrins in ambient air.

Keywords: fluorine · heterocycles · luminescent materials · porphyrins · supramolecular chemistry

How to cite: *Angew. Chem. Int. Ed.* **2015**, *54*, 4842–4846
Angew. Chem. **2015**, *127*, 4924–4928

[1] a) Y. Murakami, J. Kikuchi, T. Ohno, O. Hayashida, M. Kojima, *J. Am. Chem. Soc.* **1990**, *112*, 7672–7681; b) F. Vögtle, E. Weber, *Angew. Chem. Int. Ed. Engl.* **1974**, *13*, 814–816; *Angew. Chem.* **1974**, *86*, 896–898; c) F. Vögtle, G. Richardt, N. Werner, *Dendrimer Chemistry*, Wiley-VCH, Weinheim, **2009**; d) C. Yang, X. M. Chen, X. Q. Lu, Q. H. Zhou, Y. S. Yang, *Chem. Commun.* **1997**, 2041–2042.

[2] a) G. H. Clever, W. Kawamura, S. Tashiro, M. Shiro, M. Shionoya, *Angew. Chem. Int. Ed.* **2012**, *51*, 2606–2609; *Angew. Chem.* **2012**, *124*, 2660–2663; b) J. K. Klosterman, Y. Yamauchi, M. Fujita, *Chem. Soc. Rev.* **2009**, *38*, 1714–1725, and references therein; c) K. E. Griffiths, J. F. Stoddart, *Pure Appl. Chem.* **2008**, *80*, 485–506; d) S. Yamada, T. Ishida, T. Nogami, *Dalton Trans.* **2004**, 898–903; e) M. J. Hannon, C. L. Painting, E. A. Plummer, L. J. Childs, N. W. Alcock, *Chem. Eur. J.* **2002**, *8*, 2225–2238; f) C. Yang, O. Elbjeirami, C. S. P. Gamage, H. V. R. Dias, M. A. Omary, *Chem. Commun.* **2011**, *47*, 7434–7436.

[3] a) C. Yang, X. Wang, M. A. Omary, *Angew. Chem. Int. Ed.* **2009**, *48*, 2500–2505; *Angew. Chem.* **2009**, *121*, 2538–2543; b) C. Yang, U. Kaipa, Q. Zhang Mather, X. Wang, V. Nesterov, A. F. Venero, M. A. Omary, *J. Am. Chem. Soc.* **2011**, *133*, 18094–18097.

[4] a) C. Yang, X. Wang, M. A. Omary, *J. Am. Chem. Soc.* **2007**, *129*, 15454 – 15455; b) R. A. Fischer, C. Wöll, *Angew. Chem. Int. Ed.* **2008**, *47*, 8164 – 8168; *Angew. Chem.* **2008**, *120*, 8285 – 8289.
[5] a) M. Jang, T. Yamaguchi, K. Ohara, M. Kawano, M. Fujita, *Chem. Asian J.* **2009**, *4*, 1524 – 1526; b) D. L. Hu, J. W. M. Bush, *Nature* **2005**, *437*, 733 – 736; c) I. A. Larmour, S. E. J. Bell, G. C. Saunders, *Angew. Chem. Int. Ed.* **2007**, *46*, 1710 – 1712; *Angew. Chem.* **2007**, *119*, 1740 – 1742; d) K. Kasai, M. Aoyagi, M. Fujita, *J. Am. Chem. Soc.* **2000**, *122*, 2140 – 2141; e) S. Sato, J. Iida, K. Suzuki, M. Kawano, T. Ozeki, M. Fujita, *Science* **2006**, *313*, 1273 – 1276.
[6] a) X.-M. Chen, M.-L. Tong, *Acc. Chem. Res.* **2007**, *40*, 162 – 170; b) J.-P. Zhang, Y.-B. Zhang, J.-B. Lin, X. M. Chen, *Chem. Rev.* **2012**, *112*, 1001 – 1033; c) G. Yang, R. G. Raptis, *Chem. Commun.* **2004**, 2058 – 2059.
[7] C. Yang, M. Messerschmidt, P. Coppens, M. A. Omary, *Inorg. Chem.* **2006**, *45*, 6592 – 6594.
[8] a) W. Ouellette, M. H. Yu, C. J. O'Connor, D. Hagrman, J. Zubieta, *Angew. Chem. Int. Ed.* **2006**, *45*, 3497 – 3500; *Angew. Chem.* **2006**, *118*, 3577 – 3580; b) C. Y. Su, A. M. Goforth, M. D. Smith, P. J. Pellechia, H. C. zur Loye, *J. Am. Chem. Soc.* **2004**, *126*, 3576 – 3586.
[9] a) H. V. R. Dias, S. Singh, C. F. Campana, *Inorg. Chem.* **2008**, *47*, 3943 – 3953; b) M. A. Omary, C. Yang, US Patent 8343260, **2013**; c) M. A. Omary, C. Yang, *Prepr. Pap. - Am. Chem. Soc., Div. Fuel Chem.* **2009**, *54*, 158; d) C. Yang, M. A. Omary, *232nd ACS National Meeting* **2006**, INOR-930.
[10] K. Koren, S. M. Borisov, I. Klimant, *Sens. Actuators B* **2012**, *169*, 173 – 181.
[11] a) D. S. Hecht, R. J. A. Ramirez, M. Briman, E. Artukovic, K. S. Chichak, J. F. Stoddart, G. Gruner, *Nano Lett.* **2006**, *6*, 2031 – 2036; b) S. Ji, W. Wu, Y. Wu, T. Zhao, F. Zhou, Y. Yang, X. Zhang, X. Liang, *Analyst* **2009**, *134*, 958 – 965.
[12] K. M. Kadish, K. M. Smith, R. Guilard, *The Porphyrin Handbook*, Academic Press, San Diego, CA, **2000**, pp. 177 – 246.
[13] a) T. Yamaguchi, F. Yamazaki, T. Ito, *J. Am. Chem. Soc.* **2001**, *123*, 743 – 744; b) P. Brandi-Blanco, P. J. S. Miguel, B. Lippert, *Eur. J. Inorg. Chem.* **2012**, 1122 – 1129; c) A. Burini, J. P. Fackler, Jr., R. Galassi, T. A. Grant, M. A. Omary, M. A. Rawashdeh-Omary, B. R. Pietroni, R. J. Staples, *J. Am. Chem. Soc.* **2000**, *122*, 11264 – 11265.
[14] A. Jankowiak, D. Pociecha, J. Szczytko, H. Monobe, P. Kaszyński, *J. Am. Chem. Soc.* **2012**, *134*, 2465.
[15] a) M. A. Baldo, D. F. O'Brien, Y. You, A. Shoustikov, S. Sibley, M. E. Thompson, S. R. Forrest, *Nature* **1998**, *395*, 151 – 154; b) M. Segal, M. Singh, K. Rivoire, S. Difley, T. Van Voorhis, M. A. Baldo, *Nat. Mater.* **2007**, *6*, 374 – 378.
[16] Y. Amao, K. Asai, T. Miyashita, I. Okura, *Polym. Adv. Technol.* **2000**, *11*, 705 – 709.
[17] a) M. A. Baldo, M. E. Thompson, S. R. Forrest, *Nature* **2000**, *403*, 750 – 753; b) G. E. Jabbour, J. F. Wang, N. Peyghambarian, *Appl. Phys. Lett.* **2002**, *80*, 2026 – 2028.
[18] H. Gratz, A. Penzkofer, *Chem. Phys.* **2000**, *254*, 363 – 374.
[19] Y. Zhang, A. M. Santos, E. Herdtweck, J. Mink, F. E. Kühn, *New J. Chem.* **2005**, *29*, 366 – 370.
[20] B. R. Manzano, F. A. Jalón, I. M. Ortiz, M. L. Soriano, F. Gómez de La Torre, J. Elguero, M. A. Maestro, K. Mereiter, T. D. W. Claridge, *Inorg. Chem.* **2008**, *47*, 413 – 428.
[21] R. Galassi, S. Ricci, A. Burini, A. Macchioni, L. Rocchigiani, F. Marmottini, S. M. Tekarli, V. N. Nesterov, M. A. Omary, *Inorg. Chem.* **2013**, *52*, 14124 – 14137.

Received: November 27, 2014
Revised: January 20, 2015
Published online: March 3, 2015

